International Journal of Solids and Structures 51 (2014) 2620–2632

Contents lists available at ScienceDirect

International Journal of Solids and Structures

journal homepage: www.elsevier.com/locate/ijsolstr

A numerical model for the deterministic analysis of adhesive rough contacts down to the nano-scale

Simon Medina, Daniele Dini *

Tribology Group, Department of Mechanical Engineering, Imperial College London, South Kensington Campus, Exhibition Road, London SW7 2AZ, UK

ARTICLE INFO

Article history:
Received 20 August 2013
Received in revised form 22 January 2014
Available online 2 April 2014

Keywords:
Adhesion
Contact mechanics
Roughness
Nanoscale

ABSTRACT

A numerical model based on the Multi-Level Multi-Integration technique has been developed to study the adhesion between two surfaces. The model provides a self-consistent solution of surface separation and contact pressure throughout an arbitrary surface contact (including random surface roughness) with the adhesive interactions governed by the Lennard-Jones potential. Using this approach, the behaviour of rough surfaces can be assessed with a deterministic description of the surface, and contact stresses include valid adhesive interactions between all non-contacting surface nodes. The model is first compared to similar analyses from smooth surface models, where good agreement with published results is obtained. The model is then applied to randomly rough surfaces and shows both the significant impact of roughness on adhesive behaviour and how individual surface asperities influence the loading–unloading response of adhesive contacts. Lastly, the ability of the model to investigate nano-scale contacts is assessed through comparisons with atomistic simulations previously published elsewhere. It is clearly shown that our continuum mechanics-based model, in which an atomistic configuration is represented by a discretised continuum representation of the surface using a hard-sphere atomic model, is capable of reproducing many of the features identified through detailed atomistic simulations. The suitability of the presented model for studying adhesive contacts from the nano-scale to much larger, soft contacts, where adhesive forces can alter the contact mechanics, is demonstrated. The developed modelling tool and the algorithms implemented by the authors open the possibility to perform fast and accurate calculations using a deterministic description of the roughness for a wide variety of contact conditions.

1. Introduction

The terms adhesion or adherence are used when two bodies are stuck, or attracted to one another, and require some force to be separated. Adhesive forces are the attractive forces that can occur between two surfaces and may act between any two bodies in contact, whether or not they experience complete adherence. The presence of these adhesive forces will alter the mechanics of the contact to some extent. In many situations of interest, the effect of these adhesive forces is small compared to that of other contact forces and, consequently, can be neglected. However, this is not always the case. Two commonly cited examples are contacts between compliant (e.g. rubber) materials and contacts between bodies of nanometer dimensions. In both of these situations, adhesive forces should be accounted for in any valid contact analysis. Before returning to these examples in detail, it is useful to consider the physics of adhesive forces.

The Lennard-Jones potential, conventionally used to model simple interactions between two particles (atoms) in atomistic simulations, is also often used to describe adhesive forces in contact mechanics. The model is representative of van der Waals forces and neglects the possible influences of any electrostatic and capillary forces that may exist, but is a sensible representation for many cases of interest here. The Lennard-Jones potential is commonly expressed as:

$$V = 4\varepsilon\left\{\left(\frac{r_0}{r_s}\right)^{12} - \left(\frac{r_0}{r_s}\right)^{6}\right\} \tag{1}$$

where r_s is the separation of the two particles, r_0 is the separation at which the potential is minimum and ε indicates the strength of the interaction (the minimum potential with respect to the zero potential at an infinite separation). Differentiation of this potential with respect to r results in an expression for the force between two particles. This, in turn, can be integrated over a surface area to provide an expression that is more conveniently applied to a continuum

* Corresponding author. Tel./fax: +44 2075947242.
E-mail address: d.dini@imperial.ac.uk (D. Dini).

http://dx.doi.org/10.1016/j.ijsolstr.2014.03.033
0020-7683/

description of contact mechanics. Thus the pressure acting between two infinite, parallel surfaces separated by a distance z is given by:

$$p = \frac{8w}{3z_0}\left\{\left(\frac{z_0}{z}\right)^9 - \left(\frac{z_0}{z}\right)^3\right\} \tag{2}$$

where z_0 is the equilibrium separation, w the work of adhesion. The work of adhesion indicates the possible strength of adhesive forces between two materials; it is equal to the work required to separate two infinite surfaces from equilibrium to an infinite distance and expressed in units of energy per unit area. This force-separation curve is shown in Fig. 1, from which a number of observations can be made. Firstly, there is a maximum value of adhesive pressure acting between any two materials, whilst the repulsive pressure has no such limit. Secondly, the attractive force reaches a maximum at a separation of $(1/3)^{1/6}z_0$, and decreases rapidly as the separation increases, being just 4% of its peak value at a separation of $4z_0$. These two aspects alone can explain the circumstances in which adhesive forces can and cannot be neglected, irrespective of the type of contact and the examples given above.

Since the maximum adhesive force has a fundamental limit, the contribution of adhesion in a contact will be negligible if the applied pressure is significantly larger than this value. For this reason, the effect of adhesive forces is more evident in contacts for which the net force is low, which generally applies to smaller contacts, of order nanometers for most engineering materials. The limited range of surface separation for which adhesive forces are non-trivial also accounts for observations of low adhesion. For adhesive forces to be noticeable at the scale of the overall contact, a significant portion of the surfaces must be separated by distances within this range. Once again, this requires contacts of nanometer scale, since values for z_0 are of <1 nm. It is also apparent that contact between rough surfaces will have a greater distribution of surface gaps, which would suggest that rough surfaces will experience lower adhesion – a fact well-reported. However, the details of this phenomenon are perhaps more complex and will be examined in the later discussion.

Early research of adhesion in the field of contact mechanics included that of Bradley (1932) but it was in the 1970s that significant progress was made. Any review of the literature on adhesive contacts will highlight the acrimonious (Johnson, 1998) disagreement between proponents of two analytical models developed in this period, the JKR model (Johnson et al., 1971) and the DMT model (Derjaguin et al., 1975). Both models considered adhesive contact between a smooth sphere and a flat body, but with different approaches and making significantly different assumptions. The idea that the two models are both correct (or both incorrect) for different types of contact was put forward by Tabor (1977) who identified a characteristic parameter, now known as the Tabor parameter, of which one form is given by:

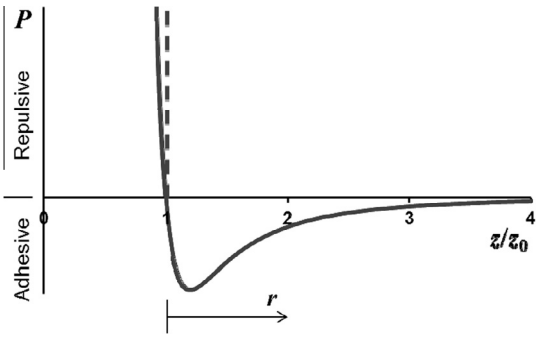

Fig. 1. Force-separation relationship for the parallel surface representation of the Lennard-Jones potential. The dashed line indicates an approximate solution for the repulsive forces.

$$\mu = \left(\frac{Rw^2}{E^{*2}z_0^3}\right)^{\frac{1}{3}}$$

where R is the radius of the sphere and E^* is the effective elastic modulus.

The JKR model was found to be representative only for contacts with a large value for the Tabor parameter ($\gg$5) and the DMT model for contacts with a small value ($\ll$0.1). This is regularly summarised by stating that the JKR model is suitable for larger, compliant contacts and the DMT for smaller, stiffer contacts. However, it must be recognised that neither model gives a full and accurate account of the contact mechanics; the assumptions made in each model become more or less valid depending upon the Tabor parameter, but each model remains an approximation of the true contact state and some local values for stress or displacement will be inaccurate. Moreover, there exists a transition region in which neither model is adequate. Muller et al. (1980) made progress in bridging the two models by removing the problematic assumptions and developing a self-consistent analysis of adhesive contact between a sphere and a flat. Greenwood later continued this approach with similar analyses to a higher level of accuracy and providing more detail of the method (Greenwood, 1997). Whilst these models seem to provide the solution to contact mechanics of smooth adhesive contacts, the complexity and numerical basis of the models hindered exploitation and alternative models were developed. Maugis applied a Dugdale-type analysis (from fracture mechanics to contact mechanics) to the problem (Maugis, 1992), replacing the true adhesive forces with a constant adhesive force acting between the surfaces at all points separated less than a critical distance. Greenwood and Johnson used a "double-Hertz" analysis to similarly simplify the solution and provide results suitable for analytical manipulation (Greenwood and Johnson, 1998). These methods may offer a step forward in analytical capabilities, but are a step back in accuracy from the Muller and Greenwood analyses, to which we will return for the development of our numerical model.

Finite element models for adhesive contact problems have also been developed, where the contact description obtained using the Lennard-Jones potential is incorporated into the framework of nonlinear continuum mechanics (Sauer and Li, 2007; Sauer and Wriggers, 2009), also in the presence of plasticity (Du et al., 2007) and within the context of multi-scale simulations, *e.g.* (Eid et al., 2011; Luan and Robbins, 2009). Alternative approaches have also been developed based on the boundary element method, which incorporates adhesion through energy minimisation (Carbone and Mangialardi, 2004; Carbone and Mangialardi, 2008).

Most of the models discussed above were developed for or applied to smooth surface contact, nominally between a sphere and a flat. Since a common justification for neglecting adhesive forces is the existence of surface roughness, a model is required that can account for the effects of surface roughness. An early and significant analysis was carried out by Fuller and Tabor (1975). Through a theoretical analysis based on an asperity model of roughness, it was shown that the adhesive influence could be described by an "adhesion parameter":

$$\theta = \frac{E^*\sigma^{\frac{3}{2}}}{\beta^{\frac{1}{2}}\Delta\gamma}$$

where β is the asperity radius, σ the *centre line average* roughness and $\Delta\gamma$ the surface energy (or work of adhesion).

This is, in effect, a ratio of the adhesive force of "lower" asperities to the elastic push of "higher" asperities. The theory was found to show reasonable agreement when fitted to experimental results. Fuller and Tabor had used the JKR model on an asperity level; Maugis repeated the analysis using the DMT model and

found an additional load would be caused by adhesive forces around each asperity (Maugis, 1996). Further advancements were made through the inclusion of elastic–plastic representation of the asperities, again based on the DMT model for asperity adhesion (Chang et al., 1988). Other attempts have been recently made to incorporate the effect of thin films (Adams et al., 2006), and to extend the validity of the maps proposed by Johnson and Greenwood (1997) to account for the strength limit (Yao et al., 2007).

Looking at other non-deterministic models of multi-asperities contacts Persson and Tosatti considered adhesion through a fractal representation of surface roughness and showed that adhesion dropped significantly at higher fractal dimensions (Persson and Tosatti, 2001). They suggested that the simpler analysis of Fuller and Tabor, and their adhesion parameter, adequately described the full detachment stage of a particle. Further discussion about the comparison between Persson stochastic roughness model and deterministic calculations is reported in Carbone et al. (2009).

These rough surface models (or asperity models) are limited to stochastic description of the surfaces and cannot provide a complete contact mechanics solution. A deterministic model is needed to compare different forms of surface roughness and investigate specific surfaces of interest. Molecular dynamics simulations of contacts can provide an extremely deterministic description of adhesive forces in a contact. Yong et al. found examples of neck formation and dislocations not identified through continuum analyses (Yong et al., 1822). Luan and Robbins demonstrated how small changes to lattice structure could alter the adhesive contact behaviour of AFM tips with a more simplified atomistic model (Luan and Robbins, 2006). Whilst it is likely such models will provide the most accurate representation of adhesive contacts in the long term, the number of atoms that can be included in a molecular dynamics simulation is limited and so only the smallest of contacts can be studied in the short term.

There is thus a need for a contact mechanics model that can provide a deterministic analysis of contact between surfaces of arbitrary shape and roughness, of small and large scale, and capable of providing accurate information for contact forces and surface displacements throughout the contact. The foundations of this model are readily found in the literature; rough surface contact models are abundant and well described. The self-consistent (locally-valid) analysis of adhesion in contacts was described by Muller et al. (1980). In the following section, these foundations are expanded upon and a method by which they can be used to model contact between rough surfaces with adhesion is described. We then verify this model through comparisons with the smooth-sphere analyses performed by Greenwood (1997) before putting the model to full use with examples of contact between rough surfaces where adhesion may or may not play a role. Finally, we examine how the continuum-founded model can be applied to the smallest contacts where atomic-scale features are important – comparisons with atomistic simulations of AFM tips by Luan and Robbins (2006) are presented.

2. Model

The model is derived from a rough surface contact solver developed by the authors and presented in Medina et al. (2012), which was based on an original methodology developed by Venner and Lubrecht (2000). The model uses the Multi-Level Multi-Integration (MLMI) technique to solve for the contact pressures for an arbitrary surface described by a uniform rectangular mesh of surface profile data. Further details can be found in Venner and Lubrecht (2000), but most of the assumptions made within this model extend to the current adhesive model:

(1) The surfaces can be described by a composite roughness, which combines the roughness and macro-geometry of both surfaces. Each node in the surface mesh is therefore assigned a height value, h, equal to the separation between the two non-deformed (rigid) surfaces at the point of first contact.
(2) Both bodies are homogeneous and elastic, and can be represented by an effective elastic modulus, E^*.
(3) The pressure at each node is taken to be uniform and act over a rectangular area corresponding to the mesh spacing.
(4) The area of contact is small compared to the dimensions of the bodies, such that each body can be considered as an infinite half-space. The elastic normal displacements at a node i can then be calculated as:

$$v_i = \sum_{\text{all } j} K_{ij} p_j \tag{3}$$

where v is the normal elastic displacement and K_{ij} is the influence coefficient for the displacement of node i due to the pressure at node j.

For contact analysis in which adhesive forces can be ignored, the problem to be solved is to find a set of *positive* contact pressures that satisfy the Signorini conditions:

$$p_i > 0 | r_i = 0 \tag{4a}$$

$$p_i = 0 | r_i > 0 \tag{4b}$$

for each node, i, where r is the residual separation between the *loaded* or *deformed* surfaces and given by

$$r_i = h_i + v_i - \delta \tag{5}$$

where δ is the imposed approach of the two bodies.

Various methods have been used to solve this problem and the MLMI technique provides a fast and sufficiently accurate solution that is well suited to extending the problem to account for adhesive forces. The MLMI method uses "stacks" of grids of varying coarseness. The finest grid has a node corresponding to each node of the discretised surface. Subsequent grids halve the number of nodes in each (x, y) direction. Two aspects to the MLMI method make use of this stack. The "multi-integration" part of the method refers to the method of calculating the nodal displacements from a set of nodal pressures (Brandt and Lubrecht, 1990). The method reduces the computational time required compared to direct calculation of Eq. (3), and the routine is implemented identically in the adhesive and non-adhesive versions of the contact solver.

The MLMI method uses a distributed relaxation process in which the contact pressures are adjusted according to the current error state in an iterative process repeated until the solution converges to an acceptable tolerance. The coarser grids help in reaching a converged solution sooner; an accurate explanation of how this is achieved can be found in the book by Brandt and Lubrecht. However, modifications to this process are used and are described later. The "full multi-grid" method builds upon this multi-grid implementation by initially solving the contact on the coarsest grid before interpolating the pressure solution to the next finer grid, to be used as the initial estimate of contact pressures.

To extend the model to accurately include adhesive forces, the Lennard-Jones potential is introduced in the form of Eq. (2). Note that this form adds a further assumption to the model – adhesive pressures between nodes must be adequately described by the pressure existing between two infinite parallel surfaces at the same separation. This has been called the Derjaguin approximation (Greenwood, 1997), and is consistent with the prior assumptions of half-space geometry and composite roughness.

At this point, a distinction must be made between the continuum and atomic use of the term "surface separation". Referring

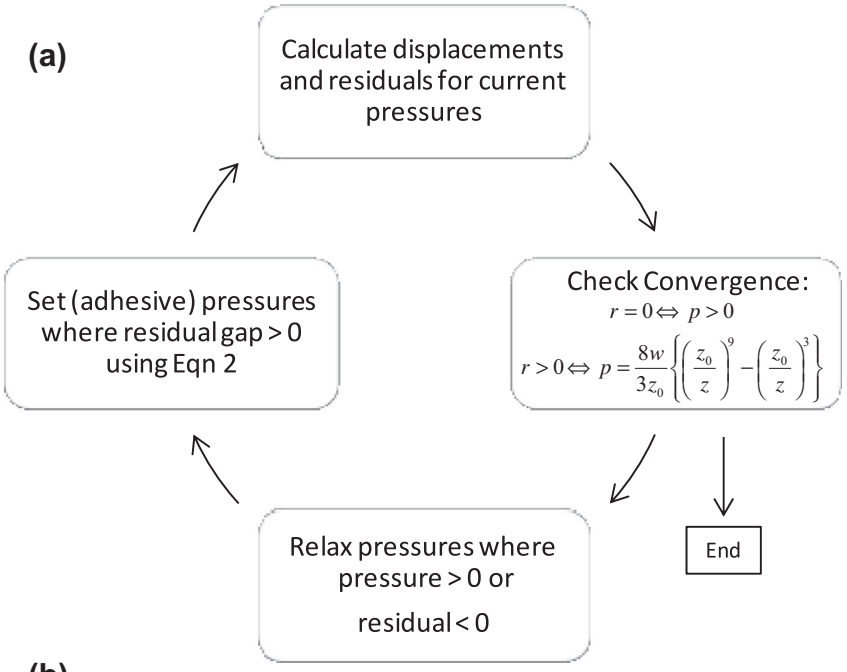

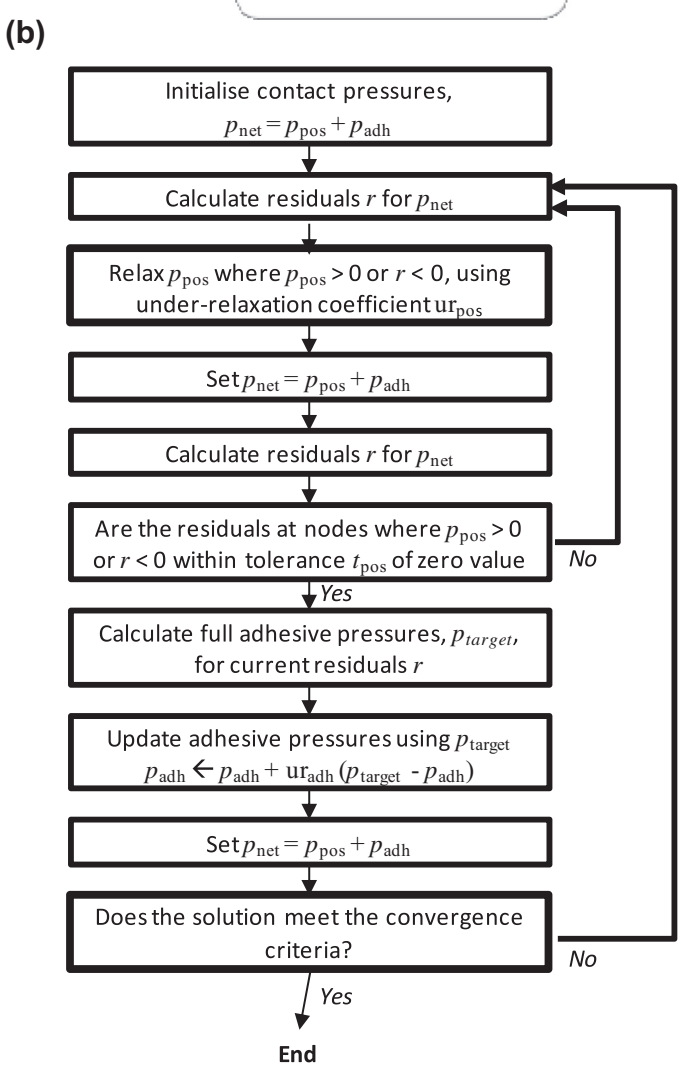

Fig. 2. Solution algorithm (a) basic, (b) modified. Wider borders summarise multiple steps.

to Fig. 1, z is the separation between surfaces in the atomic (Lennard-Jones) description of the surface. However, this separation differs from the continuum definition of separation, r, used in Eqs. (4), (5) and elsewhere. The continuum description of the surface requires zero separation ($r = 0$) wherever positive pressures exist. The atomic description, in contrast, has a finite value ($z = z_0$) at equilibrium (zero pressure) and lower values correspond to positive pressures. If the repulsive portion of the atomic force-separation curve is, temporarily, approximated by the dashed line in Fig. 1, the atomic and continuum versions of separation can therefore related by:

$$r = z - z_0 \tag{6}$$

The non-adhesive problem as described by Eq. (4) can now be reformed into an adhesive problem described by.

$$p_i > 0; \quad r_i = 0 \tag{7a}$$

$$p_i = \frac{8w}{3z_0}\left\{\left(\frac{z_0}{r_i + z_0}\right)^9 - \left(\frac{z_0}{r_i + z_0}\right)^3\right\}; \quad r_i > 0 \tag{7b}$$

Thus a further assumption has been introduced into the model, by approximating the repulsive portion of the force-separation curve. With the steep gradient of the true curve, this approximation can often be tolerated. Moreover, this approximation may be removed by replacing Eq. (7a) with:

$$p_i > 0; \quad r_i = f(p_i) \tag{8}$$

where the function f is the cubic solution for z in Eq. (2). This is, in fact, a convoluted way of describing Eq. (2) itself, but the reason for this particular formulation (Eqs. (7b) and (8)) is apparent from the solution method that follows, in which the positive pressure and adhesive portions of the contact are solved separately. With Eq. (8), the *intended* or *target* residual separation, r, becomes a function of the current nodal pressure rather than zero, but the process itself is unchanged.

Muller et al. (1980) and Greenwood (1997) obtained a self-consistent solution to Eq. (2) for a spherical contact. The solution was achieved by use of an iterative procedure involving numerical integration and elliptical integrals that could be applied to that particular geometry. As an axisymmetric problem, the solution can be described completely with respect to the distance from the contact centre and thus a 1-dimensional mesh is sufficient. Despite this relative simplification, Greenwood identified numerous difficulties in achieving convergence of the solution and obtaining complete loading and unloading data. Overcoming these difficulties in a two-dimensional, arbitrary geometry formulation is a complex challenge. Initially, a crude iteration process was implemented, as represented in Fig. 2a. This was found to work for the most favourable contacts (with very low Tabor parameter and suitable roughness), but failed to converge for most cases. Fig. 2a does, however, indicate the basic principle of the model: (1) positive pressures are relaxed with the same process as a non-adhesive contact, but with surface deformations computed with the assumed adhesive pressures included; (2) at nodes where a separation exists, the adhesive pressures are set using Eq. (2); (3) the process is repeated until the assumed adhesive pressures are converged and the residual at points of positive pressure is zero.

A number of modifications to the solution algorithm and formulation were used to improve the robustness and speed of the process. An outline of the modified algorithm is shown in Fig. 2b and some of the details follow. However, it should be noted that the process is essentially a method of obtaining a solution to the problem described by Eq. (7), and other techniques may be equally suitable.

The most obvious and problematic issue that arises from the two-dimensional, multi-asperity contact is the number of nodes required. The number of nodes must be large enough to adequately describe the pressure variation over each asperity yet be small enough to maintain an acceptable solution time. In an adhesive contact this balance is even more critical since the pressure variation of adhesive forces can be confined to a small region (requiring a fine mesh) and the iteration cycle is significantly more computationally demanding (slower) than for a non-adhesive contact. The need for sufficient nodes to describe the adhesive forces can be seen through Fig. 3, which shows an example of the surface separation and contact pressures at the edge of an asperity. If the surface separation shown by the upper black markers is assumed to exist, the nodal contact pressures obtained from Eq. (2) are represented by the blue markers. If these contact pressures are then taken to represent the uniform pressure over the element (blue lines), it is clear that the total adhesive force (the integral of the pressure profile) does not characterise the adhesive force for the true pressure profile (the black line). This is a fundamentally different problem to that of mesh refinement in non-adhesive contacts where the pressures may be blurred between nodes and fail to accurately describe the true solution. In this case, the errors can not only lead to inaccurately converged solutions but can also prevent convergence completely if the local adhesive force continues to oscillate due to the small fluctuations in the nodal separation. In order to partially overcome this problem, the expected adhesive pressure calculated for a node can be modified to better account for the full pressure integral as follows. Consider the surface profile formed by linearly interpolating the nodal values and shown by the upper black lines in Fig. 3. The pressure profile for each segment is given by Eq. (2) and this can be integrated over each linear segment as:

$$\int_{x1}^{x2} p(x)\mathrm{d}x = \int_{z1}^{z2} p(z)\frac{dx}{dz}dz = \frac{x_2 - x_1}{z_2 - z_1}\frac{4w}{3z_0}\left[\frac{z_0^3}{z_2^2} - \frac{z_0^9}{4z_2^8} - \frac{z_0^3}{z_1^2} + \frac{z_0^9}{4z_1^8}\right]$$

This integral represents the total force acting on the linear segment. Dividing this elemental force by the area of the linear segment provides a better representation of the true pressure profile, as shown by the red lines; the total adhesive force is the

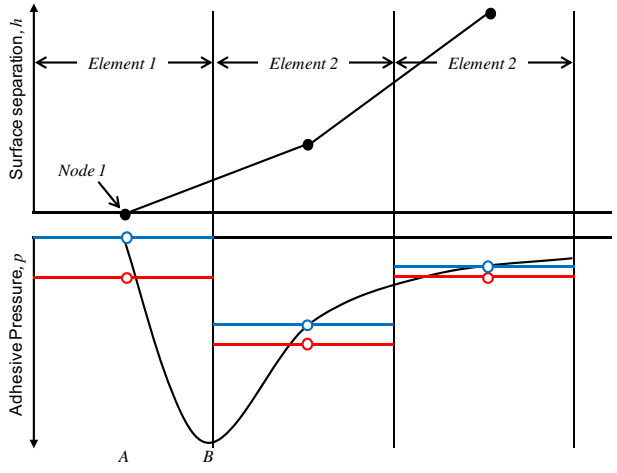

Fig. 3. Example of surface separation and pressures at a boundary between positive and adhesive pressures. The surface is described by the heights at each node. If the pressure for each element is calculated from the height at these nodes (the blue lines) then the total adhesive force is not representative of the true adhesive pressure distribution (the black curve). The red lines show the pressure allocated to each element based on the integral of the true pressure distribution for each element. (For interpretation of the references to colour in this figure legend, the reader is referred to the web version of this article.)

same irrespective of the precise location of the nodes. Therefore, instead of using Eq. (2) directly to calculate the pressure for a certain surface separation, the integral over the elemental area is taken. In two dimensions, a surface integral would ideally be employed but this is not straightforward. Instead, an average is taken of the one-dimensional integrals (defined above) for the four adjacent nodes (non-diagonal neighbours). This is able to capture the adhesion peak without significantly impacting on computa-

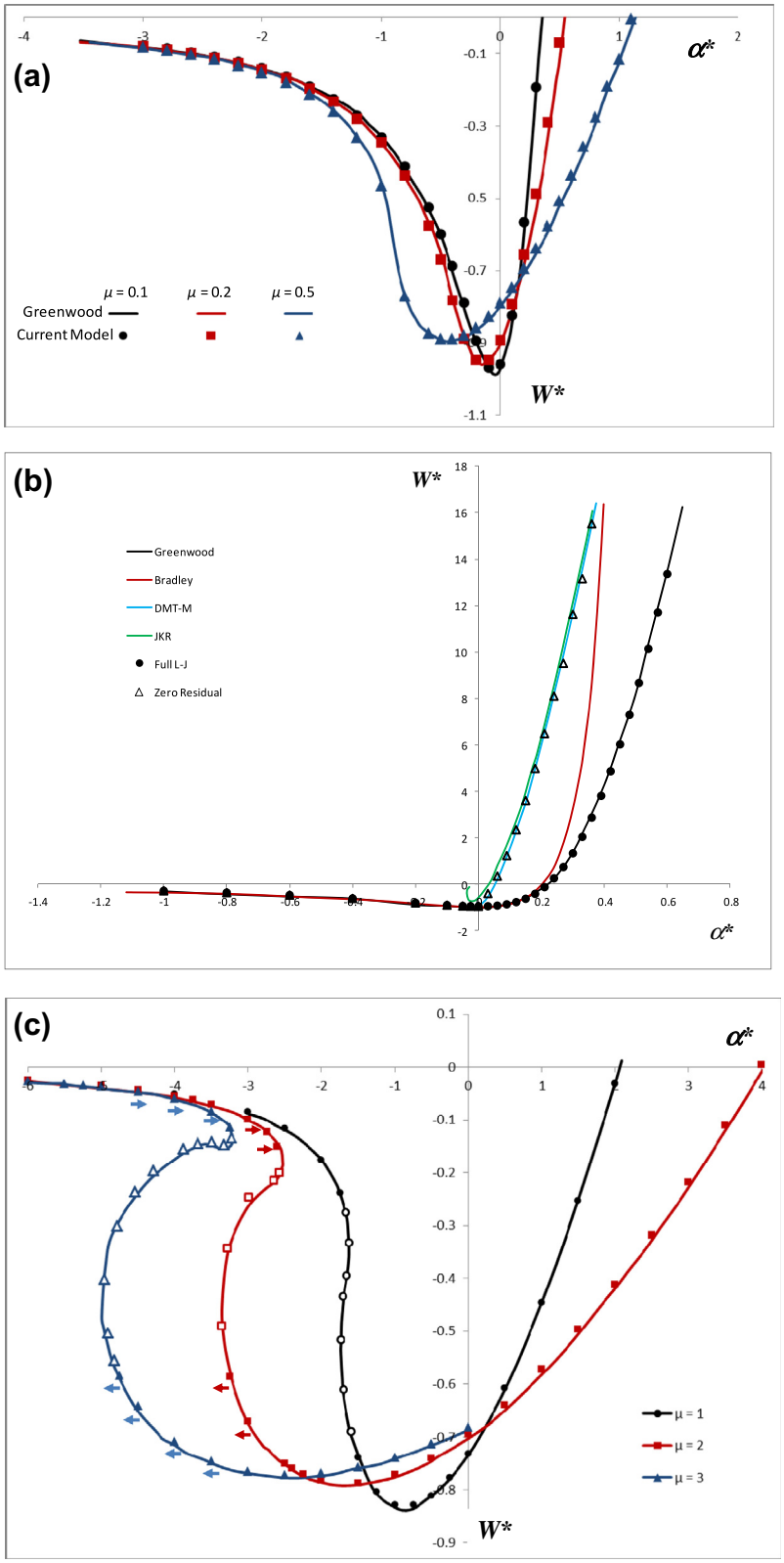

Fig. 4. Loading behaviour of a smooth spherical contact, showing comparison with results of Greenwood (1997). (a) Low Tabor parameter, (b) comparison of full and approximate representation of repulsive forces, (c) higher tabor parameter showing jump-on/off behaviour. $\alpha^* = \alpha/z_0$ is the dimensionless approach and $W^* = W/(2\pi Rw)$ is the dimensionless load.

tional performance. Finally, it must be emphasised that the mesh, ideally, would have more nodes to capture the adhesive region than those shown in the schematic presented in Fig. 3.

In the process of relaxing contact pressures, a relaxation coefficient is chosen to aid convergence. In the algorithm of Venner and Lubrecht this is chosen as a constant; they report data showing speed and accuracy of convergence for different values. Too high a relaxation coefficient can lead to divergence and a failure to find a solution; too low a value can lead to prolonged solution times. Our algorithm for non-adhesive contact utilised a method for monitoring the solution progress and adjusting the relaxation coefficient accordingly. The algorithm developed was found to provide a reasonably fast and highly robust route to obtaining a converged solution. For the adhesive version, there are two distinct relaxation processes requiring two separate, and unrelated, relaxation coefficients. These were independently monitored and optimised. However, this approach required an additional modification to the basic solution routine. To ensure that the adhesive (negative) and contact (positive) pressures could be relaxed independently, adhesive and contact pressures were stored independently and summed only upon calculating the resultant displacements. This technique was found to improve the ability to relax the adhesive pressures consistently. Additionally, the relaxation of the positive pressures was repeated until convergence within each adhesive iteration cycle; this was found to be necessary since small changes in residuals can lead to significant changes in adhesive pressures.

The final, and perhaps most critical, issue that must be addressed is the means of assessing convergence. This, again, has two components: convergence of the positive pressure relaxation process and convergence of the overall adhesive contact solution.

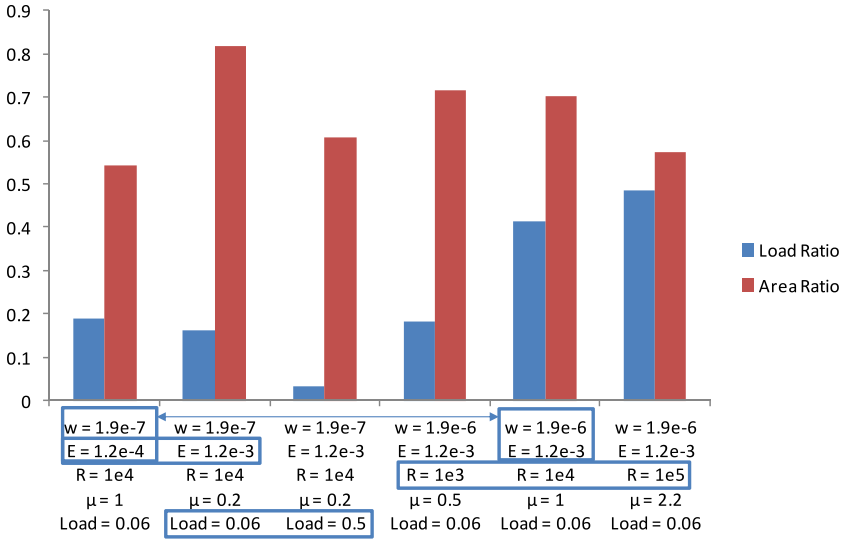

Fig. 5. Load ratio and area ratio for different contact configurations showing the relative importance of adhesion in smooth spherical contacts.

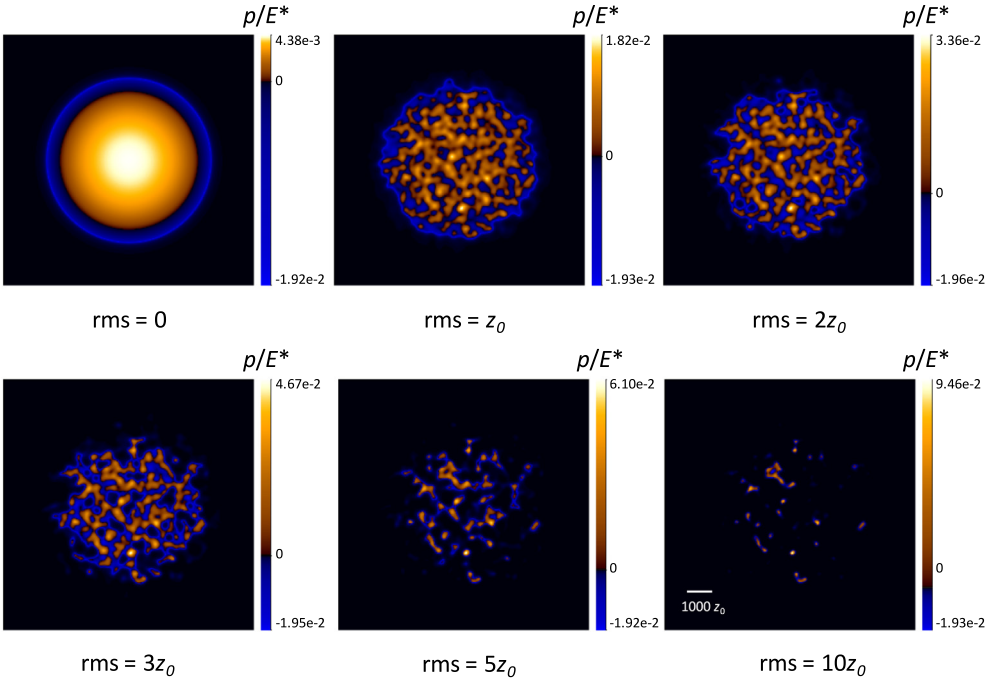

Fig. 6. Contact pressures for a smooth and rough surfaces of different rms at the same net load.

Convergence of the positive pressures was identified using the surface error rms used in Medina et al. (2012), that is the rms of the residual at each node where the net pressures is positive. It was found that a very small tolerance was required for the positive pressures and a value of 0.0001 z_o was typically used. A higher error tolerance would lead to reasonably small changes in residual separation but significant variations in the corresponding "target" adhesive pressure. For overall convergence, a criterion was required that examines the self-consistency of the current solution. The criterion applied here compares the surface residuals of the assumed solution with the residuals that would be obtained if the adhesive pressures were replaced with the exact values corresponding to the current residuals (through Eq. (2)). The process to quantify the error is thus:

(1) Obtain the surface residuals at each node, r_i, using the assumed solution pressures.
(2) Calculate the true adhesive pressures that should exist at each node given the current surface residual, r_i.
(3) Temporarily replace the trial solution adhesive pressures with those calculated in step 2, and calculate new residuals, r', using this pressure distribution.
(4) Calculate the rms of the change in residuals: $E_{\text{Total}} = \sqrt{\sum (r_i - r_i')^2 / n}$.

A convergence criterion of 0.0001 z_0 was sought for all analyses; in some cases this was could not be achieved without further mesh refinement, and the solution was taken upon the total error reaching a steady value. In all these cases, the error rms remained less than 0.001 z_0.

3. Analysis

3.1. Smooth surfaces

The model was initially verified through comparisons with the work of Greenwood, which used the same self-consistent force-seperation criteria and Lennard-Jones interaction relationship as our model, albeit in a form limited to spherical contacts. The model was used with both forms of positive pressure requirement – zero overlap (Eq. (7a)) and the full Lennard-Jones (L–J) curve (Eq. (8)). Fig. 4 shows comparisons with our models using the full L–J curve and the results presented in Greenwood (1997). Fig. 4b shows a comparison between the zero-overlap approximation and the full L–J curve solution. It is clear that using the full L–J curve gives results which match the full solution of Greenwood. Interestingly, the use of zero overlap corresponds to the DMT solution in this example. This is a result of the assumptions of the Hertzian contact solution (upon which the DMT model is based), in which there is also a requirement of zero separation at points of contact. With the low Tabor parameter value of 0.02 in the case shown, the DMT model is valid and no further differences are caused by the model's additional approximations.

In Fig. 4a and b, the full loading cycle was obtained directly as described above. However, as the Tabor parameter increases, the loading process becomes more complex, and the load-approach curve forms an S shaped region (Fig. 4c). Greenwood describes how this behaviour will manifest in practise: the contact will jump from one portion of the loading curve to another in a manner dependent upon the form of loading (load or displacement controlled) and the test-rig stiffness. In order to produce the full load-approach curve, Greenwood altered the solution procedure by fixing the imposed displacement at the centre of the contact, whilst allowing the approach to vary accordingly. We have obtained similar data through the same process of fixing the displacement at the central node, and these are shown by the unshaded markers. It should be noted that this is only possible for a smooth, spherical contact, and could not be easily transferred to a rough surface contact, where the points of maximum loading may be varied and multiple. For rough contacts, the analysis as described in the previous section will reproduce the "jump on/off" phenomena described in Greenwood (1997) as though the surfaces are loaded through displacement control within a rig of infinite stiffness. The solution obtained from our model without

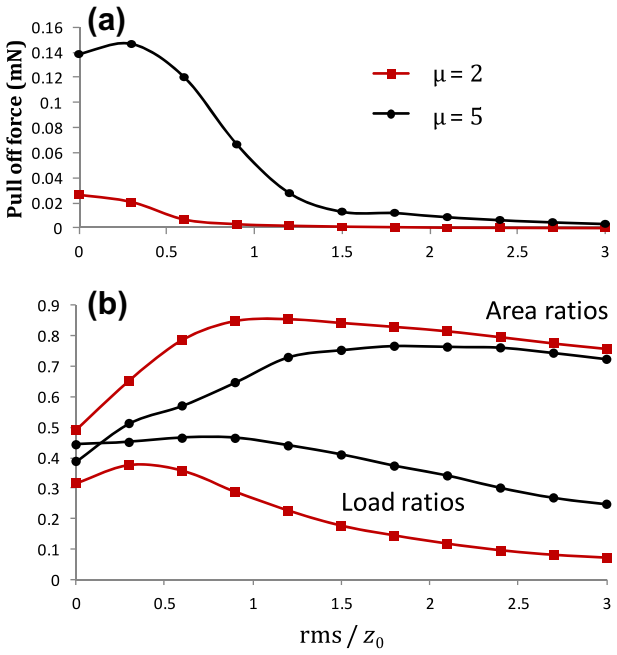

Fig. 7. Effect of roughness on (a) pull-off force and (b) adhesive load and area ratios (at a load of 0.05 mN) for two values of the Tabor parameter.

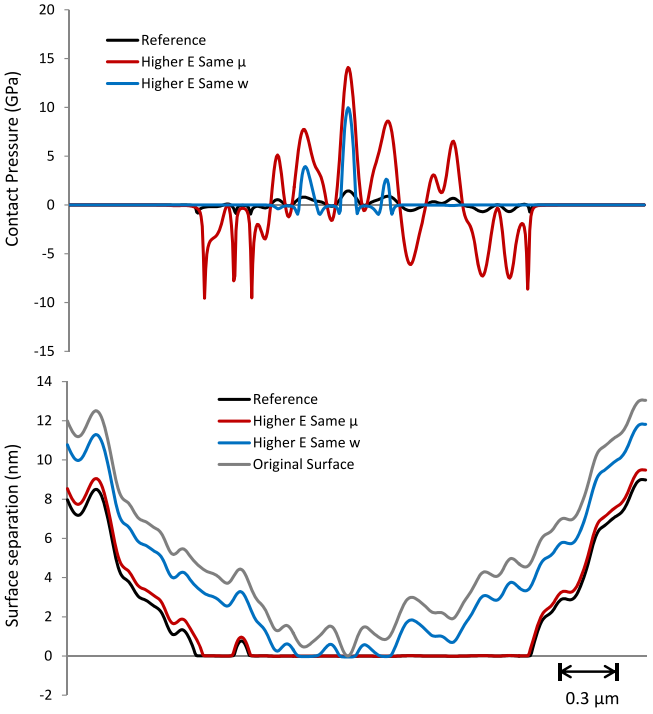

Fig. 8. Surface form and contact pressures through adhesive contacts of differing elastic modulus. The reference case is that of Fig. 6 with rms = $2z_0$.

controlling the central node separation is indicated by the filled markers in Fig. 4c. At some values of approach, two different load values are possible and occur on loading and unloading. This is produced within our model by using the contact pressures from the previous loading stage as the starting point of our iteration cycle, and this is indicated by the arrows showing the direction of loading.

At this point, it is helpful to introduce some ways to quantify the adhesive state of a contact which can then be used to assess the adhesive performance of rough surfaces. We define an adhesive load ratio as the ratio of the integral of adhesive (negative) pressures to the integral of the *modulus* of all pressures. This therefore varies between 0 and 1: an adhesive load ratio of 1 means that there are no positive contact pressures, a ratio of 0.5 means that the negative and positive pressures are equal and there is no net force between the two bodies, and 0 implies there is no adhesive force contribution. Adhesive pressures at nodes with large separations (where the adhesive pressure is less than 1% of the maximum adhesive pressure) are not included in this calculation. This ratio gives an indication of the significance of adhesion in the overall contact mechanics of the particular problem. A second indication is the adhesive area ratio, which is the ratio of nodes that have adhesive pressures, to the total number of contacting and adhesive force nodes – again neglecting those nodes at large separations and negligible adhesive pressure. Fig. 5 shows these adhesive ratios for smooth contacts of various sizes and loading conditions. Some

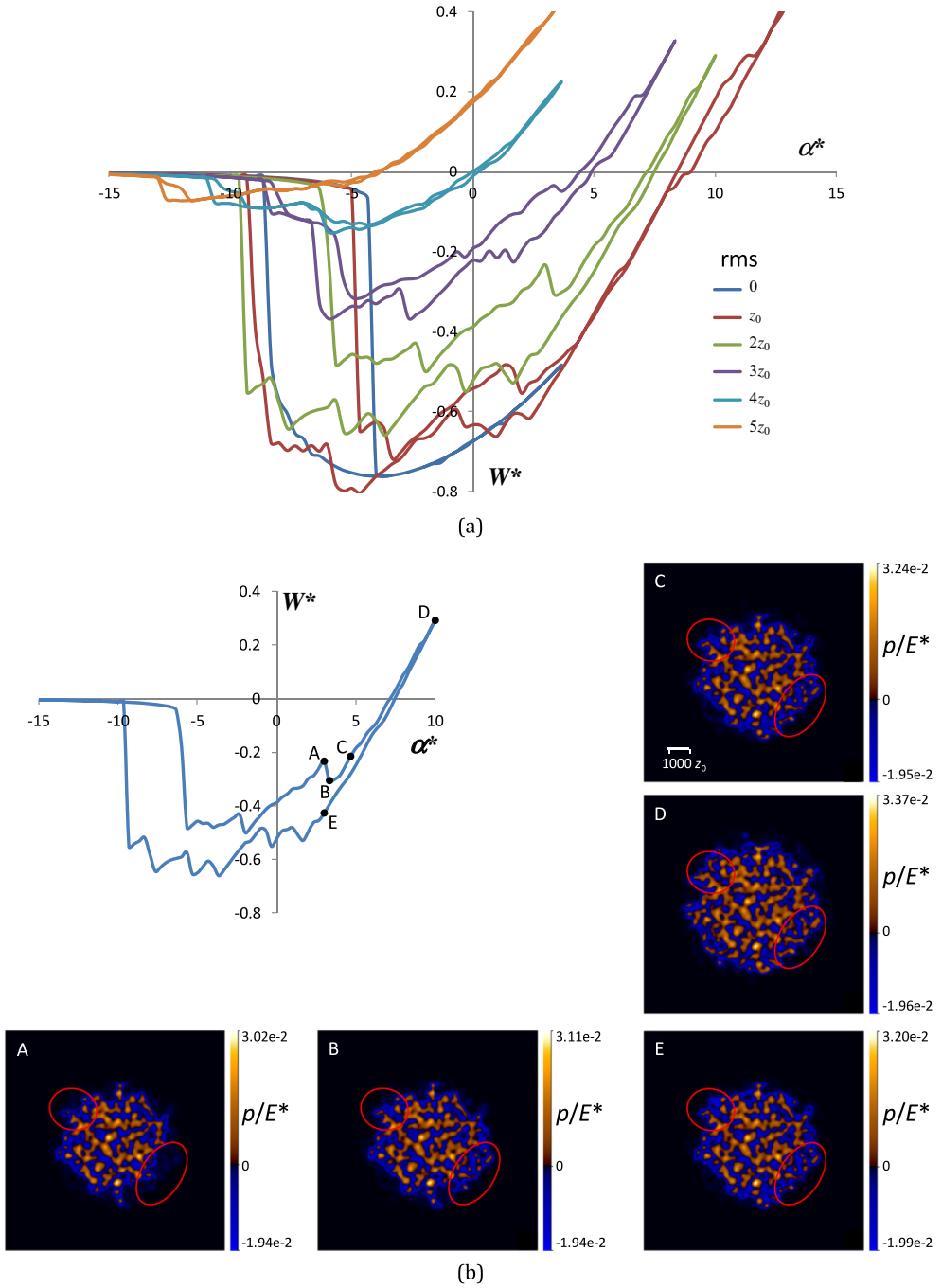

Fig. 9. (a) Loading and unloading of a rough surface for different rms. (b) Pressure distributions at different stages of loading and unloading of the rough surface with rms = $2z_0$.

comparisons can be drawn between the cases highlighted in the figure: as an example, the first two sets of results show the effect of changing the elastic modulus while maintaining the other parameters unaltered. Other cases are also indicated showing the effect of e.g. changing load or radius of curvature. One interesting comparison can be made between the first and the fifth set of results (see arrow in the inset of the figure): this shows that for contacts characterised by the same Tabor parameter, load and radius of curvature, the adhesive contribution changes depending on the magnitude of the work of the adhesion and the elastic modulus. This implies that the Tabor parameter is not sufficient (on its own) to characterise the adhesive strength of the contact.

3.2. Rough surface

Rough surfaces were numerically generated to provide a Gaussian distribution of surface heights. One particular surface was scaled in the vertical direction to produce surfaces with different rms values but identical spatial distributions of peaks and valleys. Using this technique, vertical scaling of the same random surface, enables the effect of varying roughness rms to be better isolated, and removes the variability that would be caused by the randomness of asperity locations. It must also be recognised that different rough surfaces (even with the same rms) will respond differently to adhesive loading, and results obtained from one random surface cannot be quantitatively transferred to another.

Fig. 6 shows the contact pressures for contact between a smooth sphere of radius 100 μm and the same random surface scaled to different rms for the same load of 0.05 mN ($E^* = 50$ GPa, $z_0 = 0.3$ nm, $w = 0.29$ J/m^2, giving $\mu = 5$). It has long been known that even the smallest amount of roughness can reduce adhesive forces to negligible amounts and thus we initially focus on small roughness values, of order of the atomic spacing. Fig. 7 shows the adhesive load and area ratios and for a net applied load of 0.05 mN, together with the pull-off force, as the rms is varied to 10 z_0. Initially, at very low rms values, the adhesive load increases compared to the smooth equivalent. From the pressure distribution of rms = z_0 shown in Fig. 6 it is apparent that the small amount of roughness causes a large region within the macro contact to experience a small degree of separation, where the adhesive force is maximum. This increase in adhesion with small rms was recognised by Kesari et al. (2010) and Kesari and Lew (2011). As the

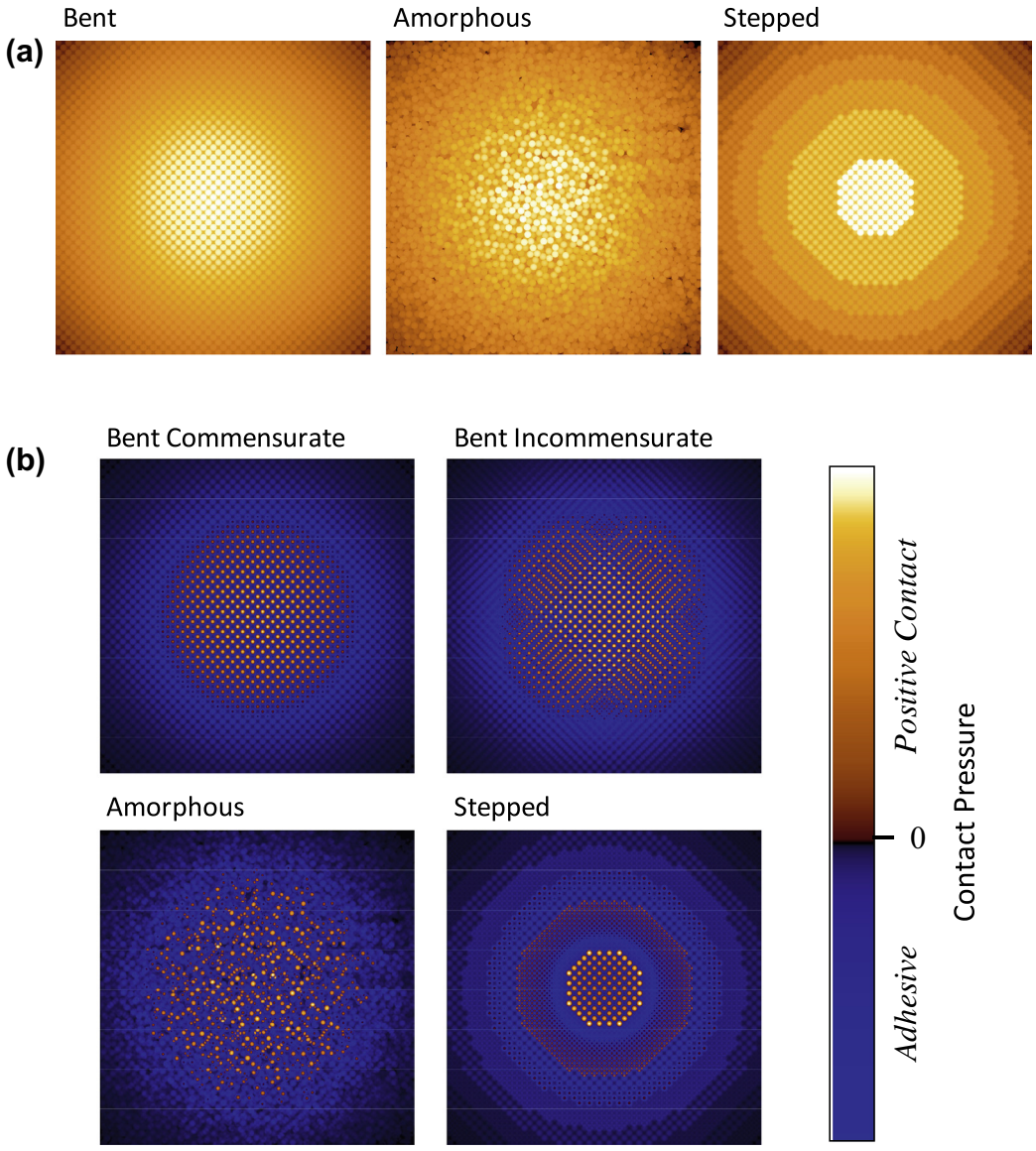

Fig. 10. (a) Discrete continuum representation of AFM tips with different atomic configurations and (b) typical contact pressures.

severity of roughness increases further, the majority of the potential contact region is separated by greater distances and experiences low adhesive forces; only local regions around positive asperity contacts are in the zone for a high adhesive force. Simultaneously, the values of the positive contact pressures increase and the relative scale of the adhesive pressures decrease (note the decreasing proportion of the blue values within the scales of Fig. 6).

Fig. 8 shows the surface form and contact pressures through a cross section of the contact represented in Fig. 6 (rms = $2z_0$) alongside similar results for a contact of higher elastic modulus only, and of higher elastic modulus and work of adhesion such that the Tabor parameter is maintained. All results are for the same load of 0.05 mN. With a high elastic modulus and identical work of adhesion, the deformed surface gradients around an asperity are steeper than for the softer (Reference, low E) material and this reduces the region over which the surface separation produces significant adhesive force. Similarly, the overall contact dimension is smaller, decreasing the average radius (and thus area) of the strongly adhesive regions. Let us now compare the results if we also increase the work of adhesion to preserve the Tabor parameter: the adhesive forces increase in strength but the contact area is still smaller than for the softer material. An alternative comparison can be made by looking at the case in which the *approach* is kept the same for each condition rather than the *load*; then, for the same Tabor parameter the deformation is such that the surface separation is identical for both the stiff and soft materials – both the contact pressures and adhesive pressures are proportionally higher for the stiff material resulting in identical separation and identical adhesive load and area ratios. This confirms that the Tabor parameter is useful in determining the form of adhesion even in rough surfaces but this only applies provided that R and z_0 are kept constant.

The jump-off and jump-on phenomena identified for smooth surfaces above are less pronounced for rough contacts. This could be expected from a simple consideration of the different scales involved as follows. The jump on/off is most significant for high Tabor parameters and thus contacts of larger radius, as shown in Fig. 4. Within a rough surface, the macro-contact is broken into multiple micro-asperity contacts. Each asperity therefore has a smaller effective radius and Tabor parameter than the nominal Tabor parameter of the macro-contact. In addition, the jump of each asperity will contribute only a small amount to the overall loading cycle. Since each asperity will come into contact at different stages in the loading process, this reduces the opportunity for significant adhesive "jumps" and prevents the S shaped loading curves of Fig. 4c. However, some individual asperity jumps can be identified by the differences in loading and unloading curves shown in Fig. 9a. Fig. 9b identifies some of the asperities that contribute to the loading feature identified at points A–C and E. Despite the surfaces being brought together between A-B (increasing approach), the net load has reduced due to the adhesive forces associated with the asperities on the right hand side (see circled areas in the figure). At C, the positive contact has increased sufficiently to offset this extra adhesive force and the net load returns to the value in A. As the surfaces are brought closer together, additional asperities are brought into contact (particularly those highlighted in the circled area). On unloading from D to E, the additional adhesive forces experienced at D act to maintain the asperity interaction and are such that the net load at E is more negative than at the same approach on initial loading (A).

3.3. Atomic scale contact

Since adhesion forces act on at the atomic level, the suitability of a continuum approach to modelling the behaviour should be evaluated. Molecular dynamics simulations of the contact between AFM probes have been carried out by Luan and Robbins (2006) and identified differences in adhesive contact behaviour between probe tips of different atomic form. They addressed the disparity between the time scales of atomistic and continuum simulations by performing the atomistic simulation at equilibrium, *i.e.* by allowing the system to equilibrate after every load increment before taking measurements. Each tip was described as smooth on a continuum scale, but the arrangement of atoms at the surface differed between (a) a bent commensurate tip, formed by distorting (bending) a regular cubic lattice into the required tip radius, the lattice having identical atomic spacing as the counter-surface; (b) a bent incommensurate tip formed likewise but with an incommensurate lattice spacing; (c) a tip cut from an amorphous block; (d) a tip cut from a regular cubic lattice. Whilst these are indeed smooth from a traditional continuum description, if the atomic structure is represented through a hard-sphere atomic model, the surface profile can instead be described by the uppermost edge of each surface atom, and would thus include an account of the atomic structure. The continuum representation of each tip profile is shown in Fig. 10a. Fig. 10b shows the pressure contours of each surface under loaded conditions identical to those used in Luan and Robbins (2006). Direct comparisons with the results of Luan and Robbins cannot be made in this format, but a comparison is achieved by integrating the pressure for all nodes representing a particular atom. Fig. 11 shows such a comparison. Although the configurations of the contacts are not identical, similar characteristics are shown for each tip form. The bent commensurate tip, for which the exact configuration can be determined, shows near identical results. The bent incommensurate tip shows similarities towards the edge but at the centre approaches the results of the commensurate tip; this is due to our alignment of the central atoms – different alignments would produce different results. Note that we have included atoms that contribute to the surface

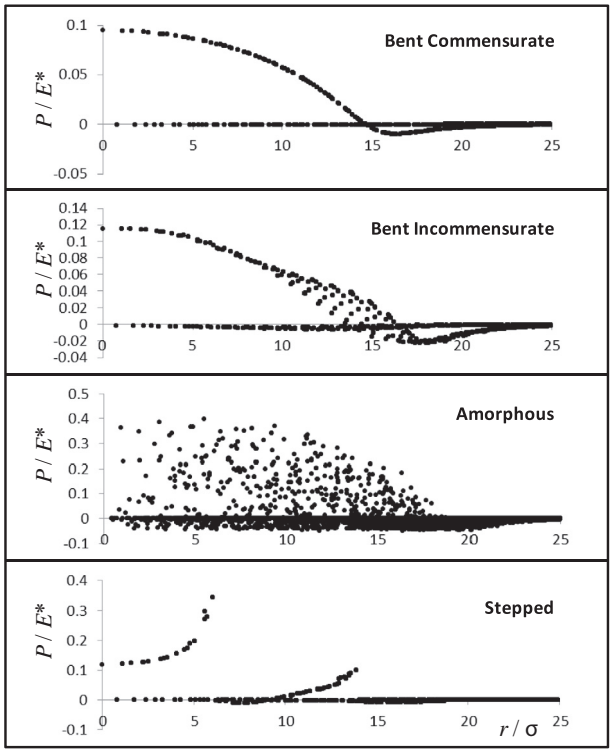

Fig. 11. Atomic force v position for different tip configuration and a comparison with results from molecular dynamics simulations (Luan and Robbins, 2006).

definition but are not within the uppermost layer of atoms, and hence many atoms with negligible adhesion can be seen at all radii – these are from the second or third layers of atoms. In comparing the different tip configurations, Luan and Robbins used two approaches: one in which the Lennard-Jones potential was kept identical for each tip and one in which the potential was varied to recreate the same work of adhesion for each tip. This highlights a complication both for experimental data analysis, and the measurement and use of values for work of adhesion. The work of adhesion used within our analyses is a value appropriate to two completely smooth, flat and parallel surfaces; this representative work of adhesion may, and will, differ from the work of adhesion calculated within an analysis. The work of adhesion used as the computational input is a reference value for Eq. (2) and related to the Lennard-Jones potential. Fan et al. (2011) show how the energy and spatial parameters of the Lennard-Jones equation, ε and r (Eq. (1)) are related to those in Eq. (2) (w and z_0); we have used work of adhesion values calculated in this manner, thus:

$$z_0 = \sqrt[6]{\frac{2}{15}} r_0$$

$$w = \frac{9\varepsilon}{2\pi z_0^2}$$

Fig. 12 shows radius and pull-off curves for each tip and ranks the effective work of adhesion for each tip (the area under the pull-off curve load axis) in the same order as Luan and Robbins. A more exact match would be unexpected since our atomic configurations are not identical, but the degree to which the quantitative results differ suggest that the continuum description does indeed provide a suitable representation of nano-scale contact problems.

4. Discussion

Analysis of a series of rough surface contacts has directly quantified the contribution of adhesive forces as the scale of the roughness varies, and how this is dependent upon the Tabor parameter. The two-dimensional contour plots of contact pressures help explain more directly the reason for this behaviour. Tabor describes rough surface adhesion as a competition between the elastic asperities pushing the surfaces apart and the adhesive forces pulling the surfaces together. It is suggested that as the roughness increases, the surfaces are pushed further apart and the adhesive forces reduced. The effect of increasing the compliance of the bodies is often described as allowing the surfaces to form around the asperities and so mitigate their effect of reducing adhesion. Whilst these facts are indeed true, these effects can perhaps be attributed more directly to the local gradient of the surfaces around asperities (or zones of positive contact pressure). For adhesive forces to have any significant influence on the contact, a sizeable area of the contact must be separated by distances of less than around $4z_0$ and this is achieved when the surface separation gradient is small. This is visible in Fig. 8, where the surface gradi-

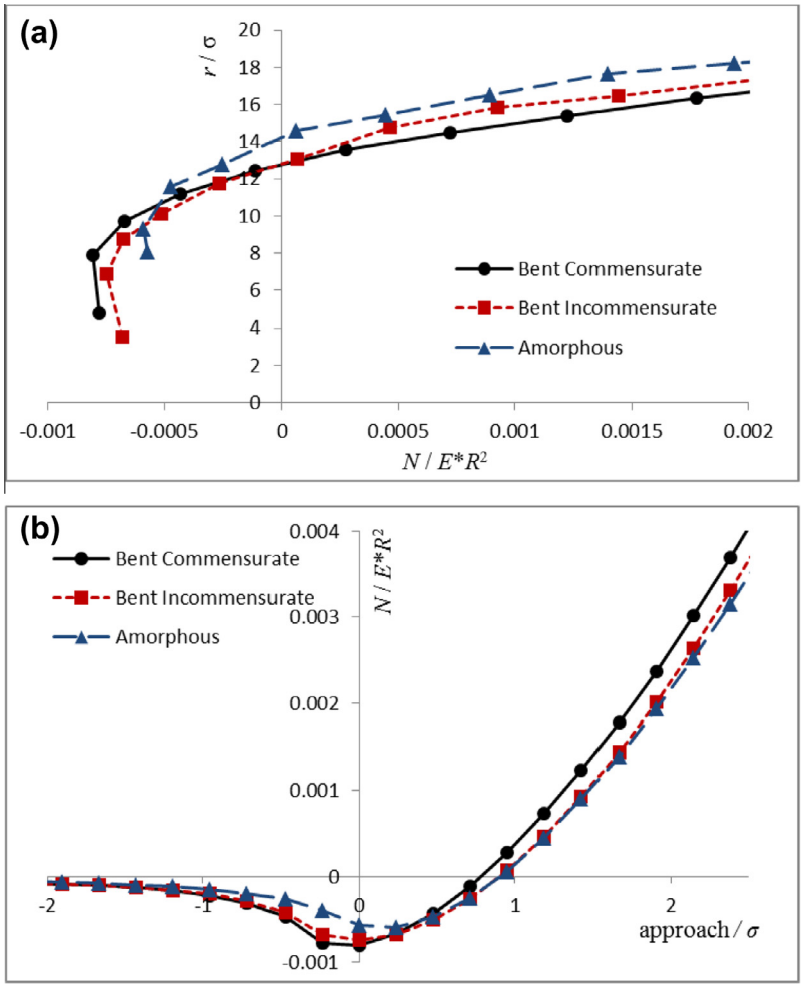

Fig. 12. (a) Contact radius vs. load, and (b) pull-off curves for different tip configurations.

ents around each contact patch is shallower for the lower modulus reference case. A small roughness value also promotes this shallow gradient around asperity contacts. Low elastic modulus also has the effect of increasing the size of each asperity contact (for a given load) and thus increasing the effective radius at which the annulus of adhesive forces occurs and thus also the area of high adhesive force and the contribution of adhesion.

Another factor that can be considered is that the adhesive forces that occur on initial contact are capable of altering the deformed profile and thus contact area. These initial adhesive forces act to pull the surfaces closer and create more regions of high adhesive force (as occurs for jump-on). This effect is clearly amplified for low modulus materials, for which the relatively low adhesive forces can significantly alter the surface profile. The effect of adhesive contact area on the overall contribution of adhesion is evident in Fig. 6, where the surfaces of roughness z_0 and 2 z_0 have a greater adhesive contribution than the smooth surface.

Despite being founded on a continuum model of elasticity, the model has shown good agreement with molecular dynamics simulations of atomic scale contacts. The use of a hard-sphere continuum description of an atomic structure enables the geometric effect of atom positioning to be captured sufficiently well to represent much of the atomic level interactions. Although the model is not capable of identifying the tangential and plastic behaviour of adhesive contacts that molecular simulations allow in its present form, it is better suited to larger scale contacts that would be overly demanding for current computational limits of MDS. Values for work of adhesion, both from an experimental and modelling aspect, must be identified with some consideration. As shown in the atomistic analyses of Luan and Robbins (2006), a given interatomic potential can results in different calculated values of work of adhesion depending upon the exact surface form. The work of adhesion used in Eq. (2) is based upon a particular calculation from the L–J potential and for perfect parallel surfaces; thus the value for w in Eq. (2) will differ from the calculated "work of adhesion" defined as the energy to separate two particular surfaces. Similarly, experimental determination or use of work of adhesion values must also account for the particular surface form, and clearly distinguish between material and surface effects.

Finally, in its current form, the model is particularly well suited to analyse rough contacts and smooth contacts with low Tabor parameter. However, low under-relaxation coefficients are needed for contacts of high Tabor parameter, therefore requiring larger computational costs in order to guarantee convergence. Furthermore, the incorporation of tangential loading and plasticity is part of our ongoing effort to study the effect of adhesion on the frictional response of rough contacts.

5. Conclusions

The effect of surface roughness on the adhesive behaviour of contacts has long been understood. It has been described qualitatively (Fuller and Tabor, 1975) and quantitatively with a stochastic view (Maugis, 1996; Chang et al., 1988; Persson and Tosatti, 2001), but the current model allows a deterministic analysis of known rough surface geometries. It is possible to examine the localised stresses and surface displacements which can be of benefit to experimental studies of nano-scale and soft contacts by shedding some light on the mechanisms responsible for hysteresis in adhesive contacts. The model is also able to compare different forms of surface roughness to a level that simple analytical or fractal-type asperity models cannot. The results have shown excellent agreement with similar models of spherical geometry contact and comparisons with molecular dynamics simulations suggest the model is suitable for even the smallest of adhesive contacts.

Acknowledgment

The authors acknowledge the support of the UK Engineering and Physical Sciences Research Council (EPSRC) via the Platform Grant EP/G026114/1.

References

Adams, G.G., Sergici, A.O., Muftu, S., 2006. Adhesion in the contact of a spherical indenter with a layered elastic half-space. J. Mech. Phys. Solids 54 (9), 1843–1861.
Bradley, R.S., 1932. The cohesive force between solid surfaces and the surface energy of solids. Philos. Mag. Ser. 7 13 (86), 853–862.
Brandt, A., Lubrecht, A.A., 1990. Multilevel matrix multiplication and fast solution of integral equations. J. Comput. Phys. 90 (2), 348–370.
Carbone, G., Mangialardi, L., 2004. Adhesion and friction of an elastic half-space in contact with a slightly wavy rigid surface. J. Mech. Phys. Solids 52 (6), 1267–1287.
Carbone, G., Mangialardi, L., 2008. Analysis of the adhesive contact of confined layers by using a Green's function approach. J. Mech. Phys. Solids 56 (2), 684–706.
Carbone, G., Scaraggi, M., Tartaglino, U., 2009. Adhesive contact of rough surfaces: comparison between numerical calculations and analytical theories. Eur. Phys. J. E 30 (1), 65–74.
Chang, W.R., Etsion, I., Bogy, D.B., 1988. Adhesion model for metallic rough surfaces. J. Tribol. 110 (1), 50–58.
Derjaguin, B.V., Muller, V.M., Toporov, Y.P., 1975. Effect of contact deformations on the adhesion of particles. J. Colloid Interface Sci. 53 (2), 314–326.
Du, Y., Chen, L., McGruer, N.E., Adams, G.G., Etsion, I., 2007. A finite element model of loading and unloading of an asperity contact with adhesion and plasticity. J. Colloid Interface Sci. 312 (2), 522–528.
Eid, H., Adams, G.G., McGruer, N.E., Fortini, A., Buldyrev, S., Srolovitz, D., 2011. A combined molecular dynamics and finite element analysis of contact and adhesion of a rough sphere and a flat surface. Tribol. Trans. 54 (6), 920–928.
Fan, K.-Q., Jia, J.-Y., Zhu, Y.-M., Zhang, X.-Y., 2011. Adhesive contact: from atomistic model to continuum model. Chin. Phys. B 20 (4).
Fuller, K.N.G., Tabor, D., 1975. The effect of surface roughness on the adhesion of elastic solids. Proc R. Soc. London Ser. A Math. Phys. Sci. (1934–1990) 345 (1642), 327–342.
Greenwood, J.A., 1997. Adhesion of elastic spheres. Proc. R. Soc. London Ser. A Math. Phys. Eng. Sci. 453 (1961), 1277–1297.
Greenwood, J.A., Johnson, K.L., 1998. An alternative to the Maugis model of adhesion between elastic spheres. J. Phys. D Appl. Phys. 31 (22), 3279.
Johnson, K.L., 1998. Mechanics of adhesion. Tribol. Int. 31 (8), 413–418.
Johnson, K.L., Greenwood, J.A., 1997. An adhesion map for the contact of elastic spheres. J. Colloid Interface Sci. 192 (2), 326–333.
Johnson, K.L., Kendall, K., Roberts, A.D., 1971. Surface energy and the contact of elastic solids. Proc. R. Soc. London Ser. A Math. Phys. Sci. 324 (1558), 301–313.
Kesari, H., Lew, A.J., 2011. Effective macroscopic adhesive contact behavior induced by small surface roughness. J. Mech. Phys. Solids 59 (12), 2488–2510.
Kesari, H., Doll, J.C., Pruitt, B.L., Wei, C., Lew, A.J., 2010. Role of surface roughness in hysteresis during adhesive elastic contact. Philos. Mag. Lett. 90 (12), 891–902.
Luan, B., Robbins, M.O., 2006. Contact of single asperities with varying adhesion: comparing continuum mechanics to atomistic simulations. Phys. Rev. E Stat. Nonlinear Soft Matter Phys. 74 (2), 026111.
Luan, B., Robbins, M., 2009. Hybrid atomistic/continuum study of contact and friction between rough solids. Tribol. Lett. 36 (1), 1–16.
Maugis, D., 1992. Adhesion of spheres: the JKR-DMT transition using a dugdale model. J Colloid Interface Sci. 150 (1), 243–269.
Maugis, D., 1996. On the contact and adhesion of rough surfaces. J. Adhes. Sci. Technol. 10 (2), 161–175.
Medina, S., Olver, A.V., Dini, D., 2012. The influence of surface topography on energy dissipation and compliance in tangentially loaded elastic contacts. J. Tribol. 134 (1).
Muller, V.M., Yushchenko, V.S., Derjaguin, B.V., 1980. On the influence of molecular forces on the deformation of an elastic sphere and its sticking to a rigid plane. J. Colloid Interface Sci. 77 (1), 91–101.
Persson, B.N.J., Tosatti, E., 2001. The effect of surface roughness on the adhesion of elastic solids. J. Chem. Phys. 115 (12), 5597–5610.
Sauer, R.A., Li, S., 2007. An atomic interaction-based continuum model for adhesive contact mechanics. Finite Elem. Anal. Des. 43 (5), 384–396.
Sauer, R.A., Wriggers, P., 2009. Formulation and analysis of a three-dimensional finite element implementation for adhesive contact at the nanoscale. Comput. Meth. Appl. Mech. Eng. 198 (49–52), 3871–3883.
Tabor, D., 1977. Surface forces and surface interactions. J. Colloid Interf. Sci. 58 (1), 2.
Venner, C.H., Lubrecht, A.A., 2000. Multilevel Methods in Lubrication. Elsevier, Amsterdam.
Yao, H., Ciavarella, M., Gao, H., 2007. Adhesion maps of spheres corrected for strength limit. J. Colloid Interface Sci. 315 (2), 786–790.
Yong, C.W., Kendall, K., Smith, W., 1822. Atomistic studies of surface adhesions using molecular-dynamics simulations. Philos. Trans. 2004 (362), 1915–1929.